Polymer Testing 97 (2021) 107162

Contents lists available at ScienceDirect

Polymer Testing

journal homepage: http://www.elsevier.com/locate/polytest

A simple design of mechanically robust, recyclable, and biodegradable composite films with high thermal stability and fluorescent properties

Jiongjiong Li [a,*], Shuaicheng Jiang [a], Ying Zhou [a], Xiaona Li [a], Sheldon Q. Shi [a,c], Jianzhang Li [a,b,**]

[a] Co-Innovation Center of Efficient Processing and Utilization of Forest Resources, College of Materials Science and Engineering, Nanjing Forestry University, Longpan Road 159, Xuanwu District, Nanjing 210037, China
[b] Ministry of Education Key Laboratory of Wooden Material Science and Application, Beijing Key Laboratory of Wood Science and Engineering, College of Materials Science and Technology, Beijing Forestry University, Beijing 100083, China
[c] Department of Mechanical and Energy Engineering, University of North Texas, Denton, TX, 76203, USA

ARTICLE INFO

Keywords:
Soy protein
Tough and strong films
Recyclable and biodegradable
High thermal stability
Fluorescent properties

ABSTRACT

It remains a big challenge to fabricate biodegradable and recyclable soy protein (SP)-based composite films with great toughness, high strength, and large ductility. In this work, a facile strategy was proposed for preparing advanced SP-based films by simple solution casting of SP and hydroxyl and primary amine-containing hyperbranched polysiloxane (HPSA). The developed SP/HPSA2 film exhibited a high toughness of 17.63 MJ m^{-3} and a high tensile strength of 15.19 MPa, which was, respectively, 424.70% and 551.93% increase compared with that of the neat SP-based film. Additionally, the SP/HPSA2 film possessed a large strain at failure of 151.01%. The advanced mechanical properties can be interpreted by the toughening and reinforcing mechanism associated with the strain-induced deformation of HPSA as well as the multiple interfacial hydrogen-bonding interactions within the interphase. The composite films exhibited great recyclability due to the reversibility of non-covalent interactions confined in the matrix. Moreover, owing to the incorporation of the heat-resistant and fluorescent HPSA, the SP/HPSA films also possessed high thermal stability and great fluorescent properties. This work offers a simple methodology for the design of mechanically robust, recyclable, and biodegradable composite films, which have potential applications in the fabrication of high-performance, high-transparency, and anti-counterfeiting packaging materials.

1. Introduction

The past few decades have witnessed such a consumption explosion in polymeric films, as they play an increasingly vital role in modern manufacturing owing to their advanced properties. Unfortunately, the rapid accumulation of non-biodegradable plastic waste has posed a pervasive threat to human health and the environment [1–4]. Accordingly, it is of permanent significance for global sustainability to prepare mechanically robust, recyclable, and biodegradable polymeric films from renewable materials.

Soy protein (SP), as the byproduct of protein industry, has drawn great attention for advanced polymeric materials due to its renewable, biodegradable, low-cost, and easily processable merits [5–7]. Ultra-stiff and strong SP-based composite films have been prepared by chemical cross-linking strategies, biomimetic structure designs, and organic-inorganic nanohybrids [8–10]. For instance, Zhang et al. prepared mechanical strong protein-based films by using cellulose nanocrystal as reinforcement and ethylene glycol diglycidyl ether as crosslinker [11]. However, the strength and ductility of polymeric films are generally mutually exclusive owing to different mechanical mechanisms. Hence, the reinforced protein-based films possessed a high tensile strength of about 5.57 MPa and a relatively low elongation at break of about 78.4%, resulting from the restraint of polymer chains mobility. Moreover, the developed composite films were unrecyclable because of the existence of covalent chemistry within the protein matrix. Therefore, it remains a long-term challenge for the fabrication of

* Corresponding author.
** Corresponding author. Co-Innovation Center of Efficient Processing and Utilization of Forest Resources, College of Materials Science and Engineering, Nanjing Forestry University, Longpan Road 159, Xuanwu District, Nanjing 210037, China.
E-mail addresses: luckyjiong@126.com (J. Li), lijzh@bjfu.edu.cn (J. Li).

https://doi.org/10.1016/j.polymertesting.2021.107162
Received 14 December 2020; Received in revised form 24 February 2021; Accepted 9 March 2021
Available online 11 March 2021

recyclable SP-based composite films with integrated high strength, large ductility, and great toughness.

Previous works have revealed that incorporating dynamic non-covalent interactions, such as metal–ligand interactions [12,13], hydrogen bonding [14,15], and hydrophobic associations [16,17], into polymers can realize the construction of recyclable composites with high strength and large extensibility. The dense non-covalent bonds can endow composites with high stiffness and strength. The dynamic rupture and re-form of such non-covalent bonds can contribute to external load energy dissipation under stress, endowing composites with good toughness and recyclability. Specifically, multiple hydrogen-bonding interactions have been proven to be the key factor to the remarkable strength and toughness of many biological materials, such as collagen fibrils and spider silk [18,19]. Super tough, strong, and remalleable polymeric films based on multiple hydrogen bonds have been reported by using poly (vinyl alcohol) (PVA) as a matrix [20]. Therefore, constructing cross-linked networks with dynamic hydrogen-bonding interactions is highly expected to be an effective strategy to prepare tough, strong, and recyclable SP-based composite films. Recently, Chang et al. adopted polyethyleneimine as plasticizer and dopamine as reinforcing agent to construct dynamic hydrogen-bonding interactions within SP matrix [5]. The developed SP-based composite films exhibited high tensile strength of 10.61 MPa, high toughness of 9.09 MJ m^3, and good self-healing properties. Nevertheless, the films were unrecyclable because of the existed covalent interactions in the protein matrix, not to mention the additives incorporated were either toxic or expensive, which goes against the tenet of green and sustainable development.

To fabricate advanced SP-based films that confined multiple sacrificial hydrogen bonds, hyperbranched polymer (HBP) with dense functional terminal groups and highly mobile external branch units is highly desirable. The flexible external segments with various end groups are highly expected to destroy the inter-/intro-molecular interactions within the SP molecules, leading to the formation of multiple hydrogen-bonding interactions between HBP and the protein matrix, as well as the increase of extensibility of the developed nanocomposites [21,22]. Additionally, both the branched structures and the internal cavities could contribute to the toughening of polymeric materials [23,24]. Amongst various HBPs, hydroxyl and primary amine-containing hyperbranched polysiloxane (HPSA) has high thermal stability, fluorescent properties, and the advantages of conventional HBP and polysiloxane [25]. Moreover, the Si–O bonds are easily rotatable, which can significantly increase the flexibility of polymer chains and facilitate the improvement of ductility. The dense hydroxyl and primary amine groups can favor the formation of multiple hydrogen bonds within the matrix, which is promising to enhance both the strength and toughness.

In this work, we propose a mechanically robust, recyclable, and biodegradable SP-based films with integrated high thermal stability and fluorescent properties simply designed by using HPSA as a toughening and strengthening agent. By solution blending HPSA with SP, cross-linked network systems confined multiple intermolecular sacrificial hydrogen bonds were formed. SP-based films with high tensile strength of 15.19 MPa, high toughness of 17.63 MJ m^{-3}, great ductility of 151.05% were fabricated. Importantly, such advanced composite films exhibited good recyclability due to the incorporated reversible non-covalent chemistry, as well as high thermal stability, fluorescent properties, and biodegradability. This work presents a facile strategy for fabricating mechanically robust, biodegradable, recyclable, and photoluminescent SP-based composite films, which can be used for preparing high-performance, high-transparency, and anti-counterfeiting packaging materials.

2. Materials and method

2.1. Materials

(3-Aminopropyl) triethoxysilane (APTES) (98.0%), 2-methyl-1,3-propanediol (MPD) (98.0%), glycerol (Gly) (99.0%), and sodium hydroxide (NaOH) (95.0%) were purchased from Aladdin Industrial Co., Ltd. (Shanghai, China), and used as received without any further treatment. SP (95% protein content) was provided by Yuwang Ecological Food Industry Co., Ltd. (Shandong, China). Deionized (DI) water was used in all experiments.

2.2. HPSA fabrication

HPSA was fabricated in accordance with the procedure reported in previous work [25]. Firstly, 1.0 mol of APTES and 1.9 mol of MPD were added into a three-necked flask with a mechanical stirrer and a thermometer under nitrogen condition. Then the mixture was heated to about 110 °C for a certain time till some distillate was distilled off. After that, the mixture was continuously heated to around 160 °C, and kept the distillate temperature below 78 °C. Finally, the hydroxyl and primary amine-containing hyperbranched polysiloxane was obtained after the distillate temperature dropped below 55 °C (Scheme 1). The obtained HPSA had a M_w of 38,577 g mol^{-1} and a PDI of about 4.32.

2.3. SP-based films preparation

Firstly, certain amount of HPSA and 1.0 g of SP powder were added into 19.0 g of DI water and stirred for 30 min. Then the pH of the SP/HPSA solution was adjusted to around 10.0 with NaOH solution (10 wt %). Next, the SP/HPSA solution was heated at 85 °C for another 30 min. After that, the SP/HPSA solution was poured into a Teflon plate (980 mm × 980 mm) and vacuum-dried at 45 °C. Finally, the films were stored in a constant temperature and humidity test chamber (25 °C and 55% relative humidity). For comparation, a neat glycerol-plasticized SP film was prepared according to previous work [5]. The preparation process was the same as that of the HPSA-modified films. The composition of the developed films is presented in Table 1. Notably, although APTES has low toxic to human health, HPSA is a relatively safe hyperbranched polymer for preparing HPSA-modified films. This is because during the fabrication of HPSA, APTES has reacted with MPD, generating ethanol as a byproduct, and the prepared HPSA possessed high molecular weight and high thermal stability. Additionally, HPSA can interact with the SP chains through multiple intermolecular interactions, leading to the formation of stable cross-linked network structures, hence HPSA couldn't migrate from the protein matrix.

2.4. Characterizations

Fourier transform infrared (FTIR) spectra of the samples were collected using a Nicolet iS50 FTIR spectrometer (Thermo Fisher Scientific, USA) ranging from 4000 to 500 cm^{-1}, aiming to characterize the changes in chemical structure of the films.

Aiming to verify the surface chemical structures of the films, X-ray photoelectron spectroscopy (XPS) was performed on an AXIS Ultra DLD instrument (Shimadzu, Japan), and Al Kα radiation was used as the X-ray source.

X-ray diffraction (XRD) patterns were obtained to characterize the conformation structures of protein, using a Rigaku Ultima IV diffractometer equipped with Cu Kα radiation source (40 kV, 40 mA), and scanned in the range of 5°–60° with a speed of 5° min^{-1}.

Dynamic mechanical analysis (DMA) spectra of the films were measured on a TA Instruments Q800 DMA system in tensile mode at a frequency of 1 Hz. The temperature was in the range of 40–240 °C at a heating rate of 5 °C min^{-1}.

Differential scanning calorimetry (DSC) curves were measured on a TA instruments DSC250 system to characterize the glass transition temperature (T_g) of the HPSA and films. The temperature was in the range of −80−180 °C at a heating rate of 20 °C min^{-1}.

Thermomechanical analysis (TMA) analysis was performed to characterize the coefficient of linear thermal expansion values of the films,

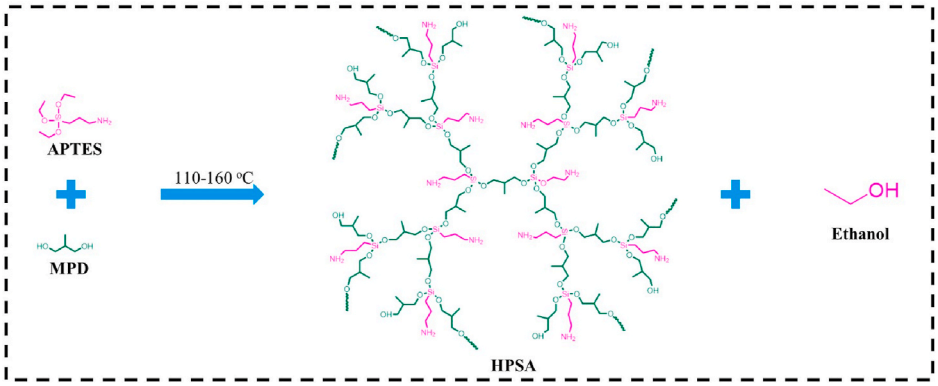

Scheme 1. The synthetic route to HPSA.

Table 1
Experimental formulations of the SP-based films.

Samples	SP (g)	DI water (g)	HPSA (g)	Gly (g)
SP/HPSA1	1.0	19.0	0.1	–
SP/HPSA2	1.0	19.0	0.2	–
SP/HPSA3	1.0	19.0	0.3	–
SP/HPSA4	1.0	19.0	0.4	–
SP/HPSA5	1.0	19.0	0.5	–
SP/Gly	1.0	19.0	–	0.5

using a TA instruments TMA Q400 system. The temperature was in the range of 30–140 °C at a heating rate of 2 °C min^{-1}.

2.5. Mechanical performance

The mechanical properties of the films (about 150 μm in thickness) were determined according to the ASTM D882-12 standard using an AGS-X-10kN electric universal testing machine (Shimadzu, Japan) at a speed of 20 mm min^{-1} [26].

2.6. Recycling performance

Firstly, the as-fabricated films were cut into pieces using a pair of scissors. Then the film pieces were redissolved in DI water by heating at 85 °C for 4 h. After a 30 min of ultrasonic treatment, the obtained solutions were poured into a Teflon plate and vacuum-dried at 45 °C to remove the water.

2.7. Thermal performance

Thermogravimetric analysis (TGA) and derivative thermogravimetric (DTG) curves were recorded on a TA instruments TGA 50 system to investigate the thermal properties of the HPSA and films. The temperature was in the range of 30–600 °C at a heating rate of 10 °C min^{-1}.

2.8. Fluorescent performance

The fluorescence intensity spectra of the films were measured using a LS-55 luminescence spectrometer (PerkinElmer, Leeds, UK). The excitation wavelength was set at 375 nm with a 10-nm slit width. For the test of 5 wt% SP solution, the excitation wavelength was set at 375 nm with a 2.5-nm slit width; the emission wavelength was set at 485 nm with a 10-nm slit width. For the test of 5 wt% HPSA solution, the excitation wavelength was set at 375 nm with a 12-nm slit width; the emission wavelength was set at 440 nm with a 12-nm slit width.

2.9. Biodegradable performance

Aqueous soil culture liquid method was used to determine the biodegradability of the prepared films according to previous works [5,22]. In brief, some outdoor soil at a depth of 2–8 cm below the ground was carefully collected and placed at a well-ventilated place for about 7 days. Next, the soil was crushed and screened through a 200-mesh sieve to remove debris. After that, 0.01 g ml^{-1} soil inoculation source was prepared by mixing certain amount of soil powder and DI water. After the films (20 mm × 20 mm) were oven-dried to constant weight, the film samples were wrapped by plastic mesh and immersed in the soil inoculation source. Finally, the weight residue of the films based on the weight ratio of the degraded film to the original film was calculated.

2.10. Statistical analysis

The statistical analyses of the data were conducted using analysis of variance (ANOVA) in the SPSS 24.0 statistical software. Differences between pairs of means were assessed using Duncan's multiple range tests ($p < 0.05$).

3. Results and discussion

3.1. Physical cross-linking network within the films

SP-based films with high optical transmittance (Fig. S1) were facilely fabricated by solution casting of HPSA and SP, as illustrated in Scheme 2. HPSA possessed a low T_g of about −60.3 °C (Fig. S2), which was positive for the increase of extensibility of the developed film [26]. The hydroxyl and primary amine groups in HPSA were highly expected to form multiple non-covalent interfacial interactions with the protein matrix, hence solving the problems of the films associated with the tradeoff between tensile strength and fracture toughness.

FTIR spectra (Fig. 1a) were used to investigate the intermolecular interactions between SP and HPSA within the films. For the FTIR spectrum of SP powder, the absorption peaks at 3274, 2929, 1633, 1515, 1394, 1234, and 1073 cm^{-1} were related to O–H and N–H bending, $–CH_3$ stretching, C═O stretching (amide I), N–H bending (amide II), COO– bending, C–N and N–H stretching (amide III), and C–O bending, respectively [24,27,28]. For the SP/HPSA films, the emergence of new absorption peaks at 1031 cm^{-1}, corresponding to the Si–O–C bonds [29], indicated the presence of HPSA molecules. After the introduction of HPSA, the peaks at 1633 cm^{-1} and 1394 cm^{-1} shifted to 1624 cm^{-1} and 1397 cm^{-1} respectively; the peaks at 1515 cm^{-1}, 1234 cm^{-1}, and 1152 cm^{-1} shifted to 1534 cm^{-1}, 1238 cm^{-1}, and 1191 cm^{-1} for SP/HPSA1, and further shifted to 1540 cm^{-1}, 1235 cm^{-1}, and 1195 cm^{-1} for the rest SP/HPSA films respectively. The absorption peaks corresponding to C–N and N–H stretching of amide III and COO– bending decreased in intensity as the addition of HPSA. These results

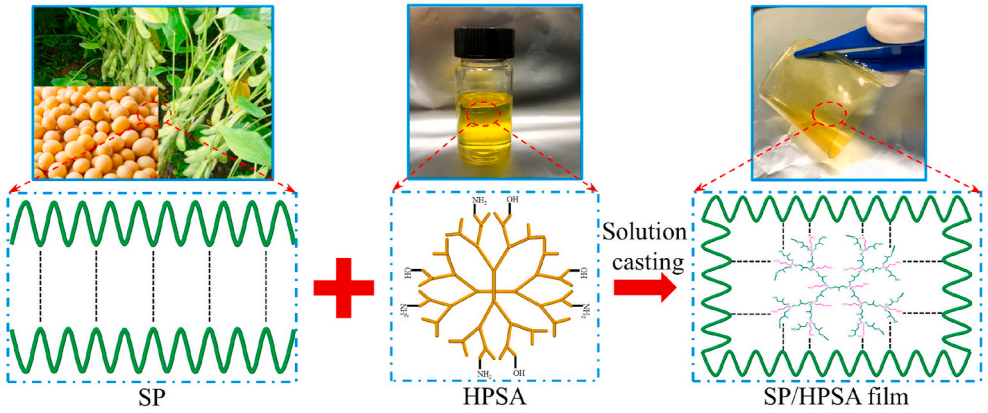

Scheme 2. Schematic diagram of the SP/HPSA film.

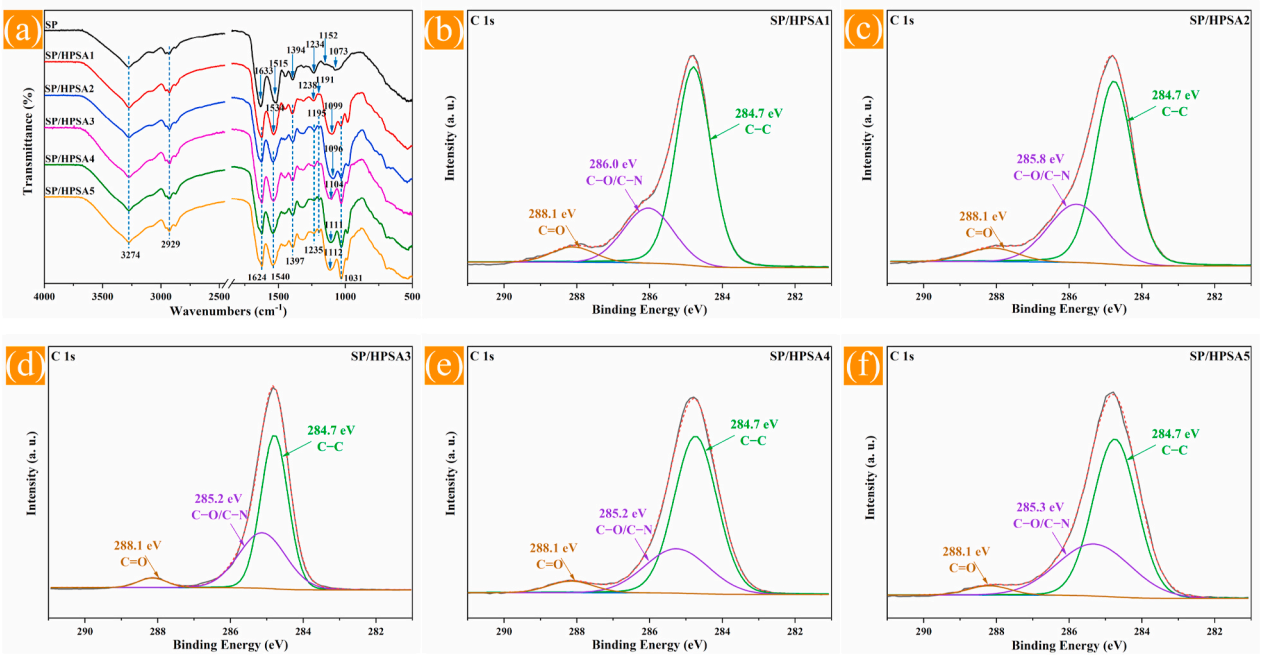

Fig. 1. (a) FTIR spectra of SP powder, SP/HPSA1, SP/HPSA2, SP/HPSA3, SP/HPSA4, and SP/HPSA5 films. Deconvolution curves of C 1s XPS spectra for (b) SP/HPSA1, (c) SP/HPSA2, (d) SP/HPSA3, (e) SP/HPSA4, and (f) SP/HPSA5 films.

were caused by the fact that the functional groups of HPSA formed multiple intermolecular hydrogen-bonding interactions with the oxygen- and amide-containing functional groups of the protein chains [27,30,31]. Additionally, the absorption peak related to the C–O bending shifted from 1073 cm^{-1} towards 1100 cm^{-1} for SP/HPSA1, and shifted towards higher wavenumbers as the increase of HPSA loading content, which further indicated that strong interfacial interactions occurred between the HPSA and SP molecules through dense non-covalent cross-linking interactions.

XPS spectra were further used to verify the surface chemical structures of the films. As shown in Fig. 1b–f and Fig. S3, there was no new peak appeared in the deconvolution curves of C 1s and N 1s XPS spectra for the developed films after the incorporation of HPSA. Additionally, all the films had a similar $–NH_2/–NH–$ ratio. These results confirmed that there were no covalent intermolecular interactions formed within the films [28]. The FTIR and XPS results led to the conclusions that the incorporation of HPSA into the films resulted in the formation of physical cross-linking networks, which comprised multiple interfacial hydrogen-bonding interactions.

3.2. Characterization of the films

The conformation structures of SP in the films were changed after the incorporation of HPSA, as shown in Fig. 2a. Compared with the SP powder, the α-helix conformation in the XRD patterns of SP/HPSA films shifted towards a lower degree and decreased in intensity, indicated the destroy of α-helix and the unfolding of the random coil in SP chains [4,28]. Additionally, the sharp diffraction peaks assigned to the β-sheet conformation became broader and the crystallinity degrees continuously decreased (Fig. S4a) as the increase of HPSA loading content. These phenomena revealed that the highly branched structures of HPSA have destroyed the crystal structures of SP molecules and interrupted the protein chains, leading to the formation of a uniform structure [28].

DSC analysis was used to investigate the changes of glass transition temperature of the developed films. The DSC curve of the SP powder exhibited two distinct glass transitions (Fig. S4b), i.e., T_{g1} = 52.26 °C and T_{g2} = 112.84 °C, which can be interpreted by the movement and denaturation of the 7S and 11S proteins [32]. For the DSC curves of the SP/HPSA films (Fig. 2b), only one endothermic transition could be observed, indicating that the added HPSA was uniformly dispersed in

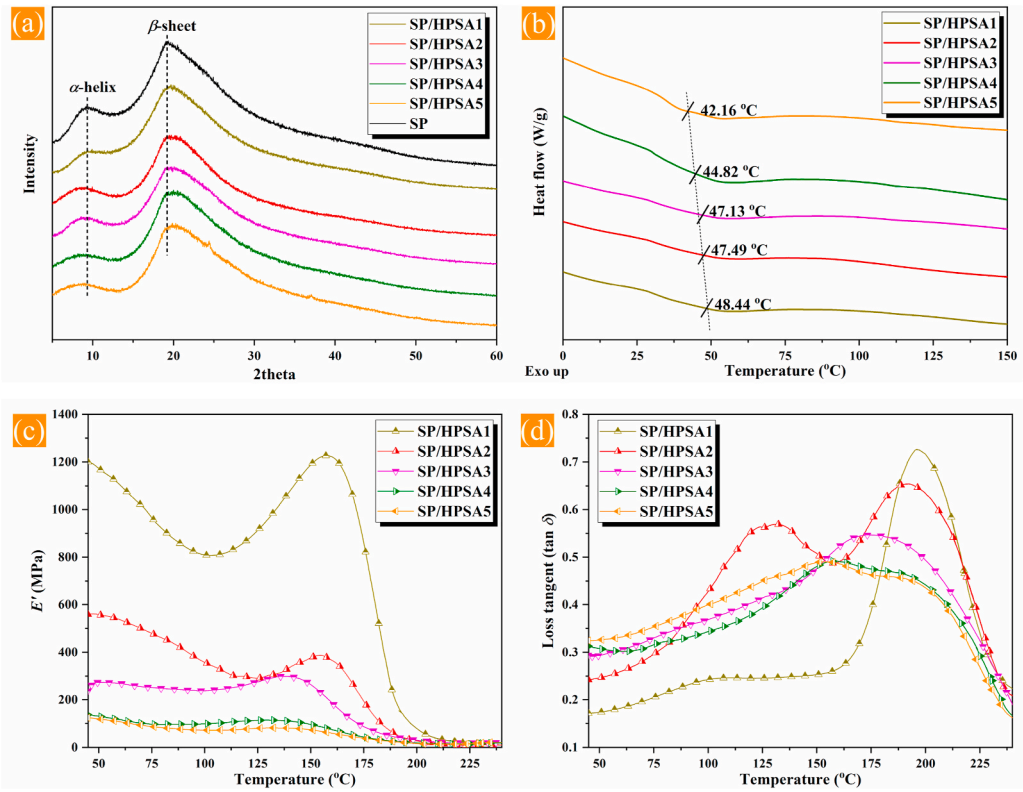

Fig. 2. (a) XRD patterns of SP powder, SP/HPSA1, SP/HPSA2, SP/HPSA3, SP/HPSA4, and SP/HPSA5 films. (b) DSC curves of SP/HPSA1, SP/HPSA2, SP/HPSA3, SP/HPSA4, and SP/HPSA5 films. (c) Storage modulus (E') and (d) loss tangent (tan δ) of SP/HPSA1, SP/HPSA2, SP/HPSA3, SP/HPSA4, and SP/HPSA5 films.

the SP matrix and a homogeneous phase system was formed [28]. Importantly, the glass transition temperatures for the SP/HPSA films decreased with the HPSA loading content, which can be interpreted by the low T_g of HPSA as well as the increased flexibility of SP-based films.

The storage modulus (E') of the developed films is given in Fig. 2c. The E' decreased as the incorporation of HPSA and the SP/HPSA5 film exhibited the lowest E'. This phenomenon could be explained by the fact that the flexible external segments of HPSA improved the plasticity of

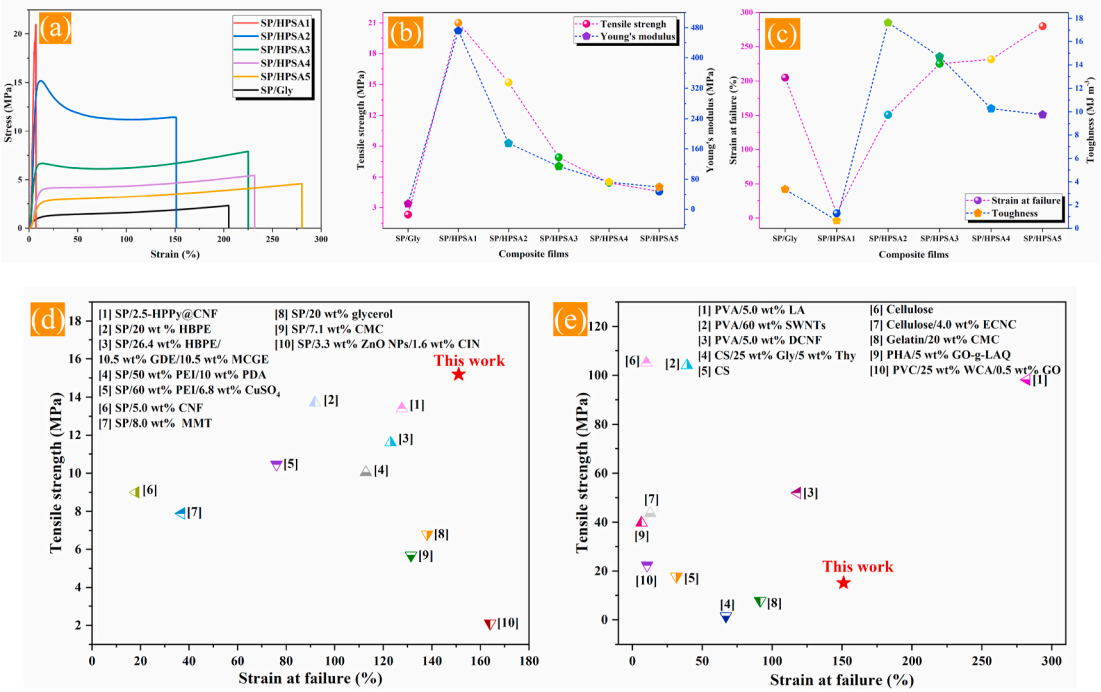

Fig. 3. (a) Engineering stress-strain curves, (b) tensile strength and Young's modulus, and (c) toughness and strain at failure of SP/HPSA1, SP/HPSA2, SP/HPSA3, SP/HPSA4, and SP/HPSA5 films. (d) Comparison of tensile strength and strain at failure of SP/HPSA2 film with other SP-based composite films [5,22,26,28,34–39]. (e) Comparison of tensile strength and strain at failure of SP/HPSA2 film with other polymeric materials [1,2,40–47].

the as-fabricated composite films by increasing the mobility of the SP chains [26]. In addition, the loss tangent (tan δ) peaks shifted towards a lower temperature with the HPSA loading content increased (Fig. 2d), further indicating the increased number of mobile SP chains [33]. It can be clearly seen that the full width at half-maximum of tan δ became broader as the increase of HPSA content, which confirmed the formation of a more uniform network structure [26]. Generally, the superhigh stiffness and brittleness of SP-based polymeric materials are mainly caused by the dense inter-/intro-molecular interactions confined in the protein molecules, and the destroy of such inter-/intro-molecular interactions can effectively increase the extensibility and toughness of the obtained nanocomposites [22]. Therefore, these results led to the conclusions that the incorporated HPSA with highly branched structures and dense terminal hydroxyl and amino groups can effectively increase the toughness and ductility of the developed SP-based composite films.

3.3. Mechanical performance

Fig. 3a gives the engineering stress-strain curves of the developed composite films and the characteristic results are listed in Table S1. Different contents of HPSA had significant effects on the mechanical properties of the films ($p < 0.05$). Compared with the SP/Gly film (control), the tensile strength and Young's modulus of the SP/HPSA films were remarkably increased. For the SP/HPSA1 film, the tensile strength and Young's modulus significantly increased to 21.00 MPa and 471.69 MPa from 2.33 MPa to 14.61 MPa for the SP/Gly film, respectively, and then decreased as the increase of HPSA loading content (Fig. 3b). Unfortunately, the strain at failure and toughness of the SP/HPSA1 film was, respectively, 6.92% and 0.67 MJ m^{-3}, which was lower than that of the SP/Gly film. These results could be caused by the low loading content of the flexible HPSA [26]. As seen in Fig. 3c, the strain at failure of the SP/HPSA films gradually increased with the HPSA loading content, which gave a strong evidence to support the plasticizing capacity of HPSA. The toughness of the fabricated films increased first and then decreased as the increase of HPSA content. The SP/HPSA2 film exhibited the highest toughness of 17.63 MJ m^{-3}, as well as a high tensile strength of 15.19 MPa and a high Young's modulus of 174.63 MPa, which was 424.70%, 551.93%, and 1095.27% increase compared with the 3.36 MJ m^{-3}, 2.33 MPa, and 14.61 MPa of the SP/Gly film, respectively. Moreover, the SP/HPSA2 film still possessed a high strain at failure of 151.01%. The remarkable mechanical properties obtained in the SP/HPSA2 film probably benefited from the physical cross-linking networks confined in the protein matrix, as well as the unique structural characteristics of HPSA.

Fig. 3d compares the tensile strength and strain at failure of the SP/HPSA2 film with other SP-based composite films. The prepared SP/HPSA2 film exhibited a far higher tensile strength and better stretchability than the other SP-based films. Although SP-based composite films with a high tensile strength of ca. 13.4 MPa and a high breaking strain of ca. 127.6% have been previously reported by integrating dopamine-containing hyperbranched poly (amino ester)-pyrrole (HPPy) decorated cellulose nanofibril (CNF) and SP [34]. Nevertheless, not to mention the tedious fabrication process, the additives incorporated were either expensive (dopamine and CNF) or toxic (dimethyl sulphoxide). In comparison, the SP/HPSA2 film was prepared via a facile and cost-effective strategy without the use of any organic solvents or other toxic reagents. Moreover, the SP/HPSA2 film also had a much greater fracture toughness (17.63 MJ m^{-3}) than the previously reported SP-based films. The comparison of tensile strength and strain at failure of the SP/HPSA2 film with other polymeric materials is shown in Fig. 3e. The developed SP/HPSA2 film exhibited higher ductility than the gelatin-, cellulose-, and CS-based composite films. Although the tensile strength of the SP/HPSA2 film was inferior to other commercial plastics, its mechanical properties still met the requirements of packaging materials [5,22].

3.4. Recycling performance

The fabricated SP/HPSA2 film was taken as an example to demonstrate its recyclability according to previous work [26], as shown in Fig. 4a. First, the SP/HPSA2 film was cut into pieces using a pair of scissors. Next, certain amount of the film pieces were redissolved in DI water to form a homogeneous film-forming solution by heating at 85 °C for 4 h. Finally, the recycled transparent film (SP/HPSA2-R) was obtained by solution casting method. The mechanical properties of the SP/HPSA2-R film is presented in Fig. 4b and c. As can be seen, although the mechanical properties of the SP/HPSA2-R film were inferior to that of the SP/HPSA film, it still exhibited a high tensile strength of 10.12 MPa, high toughness of 10.78 MJ m^{-3}, and large stretchability of 132.35%. Overall, the prepared SP-based composite films in this approach possessed complete recyclability under a mild redissolution condition as well as remarkable mechanical properties. The good recyclability of the developed composite films benefited from the multiple intermolecular reversible hydrogen-bonding interactions formed within the protein matrix [20,26]. The complete recyclability of the films could facilitate the sustainable development of polymeric materials and the settlement of environmental and energy issues arised from the increasing consumption of non-renewable fossil resources.

3.5. Toughening and reinforcing mechanism

Polymers with high molecular weight generally have large space volumes and high steric hindrance, hence they possess poor extensibility. By the incorporation of additives with larger free volumes, the polymer chain segments can occupy more free space for movement, rotation, and/or distortion, which can increase the plasticity and toughness of polymers [48]. According to the free volume theory, the free volume fraction of polymeric materials is proportional to the difference in the coefficient of volumetric thermal expansion values between the rubbery and glassy states [26]. In addition, as for an isotropic material, the coefficient of linear thermal expansion (CLTE) is about one third of the coefficient of volumetric thermal expansion [22]. Therefore, it can be concluded that the free volume fraction of polymeric materials is proportional to the difference ($\Delta\alpha$) in the coefficient of linear thermal expansion values between the rubbery (α_r) and glassy (α_g) states [22]. TMA analysis was used to determine the CLTE values of the prepared films, and the results are shown in Fig. 5 and Fig. S5. As can be seen, the α_r, α_g, and $\Delta\alpha$ values of the SP/HPSA2 film were higher than that of the SP/Gly film. This result indicated that the free volume fraction of the developed composite films increased as the incorporation of HPSA.

In light of the aforementioned results, a toughening and reinforcing mechanism of strain-induced deformation and 3D enmeshment effect of HPSA on SP matrix was proposed, as shown in Fig. 6. The incorporated HPSA was homogeneously dispersed in the protein matrix and formed multiple intermolecular hydrogen bonds with the peripheral SP chain segments. When the SP-based films were under stretching, the external load energy transferred rapidly from the protein chains to the HPSA via the dense interfacial interactions. Owing to the highly branched structures of HPSA, the stress concentrations were effectively retarded. The scattered HPSA molecules began to deform before the deformation of the SP matrix due to their higher flexibility and free volume fraction compared to the latter, and the SP chain segments that surrounded the HPSA started to rotate simultaneously. These behaviors could dissipate much external load energy and impede the emergence of microcracks. In addition, the multiple intermolecular sacrificial hydrogen bonds began to dynamically rupture and re-form, which can further absorb much load energy and enhance the fracture tolerance of the films. Under further stretching, the microcracks generated within the SP matrix and diffused towards the interfaces. Subsequently, the internal cavities of the HPSA can passivate the crack tips, and then the propagation of microcracks was blocked and terminated. Finally, when the strain extended to the breaking strain, the stretched composite films fractured.

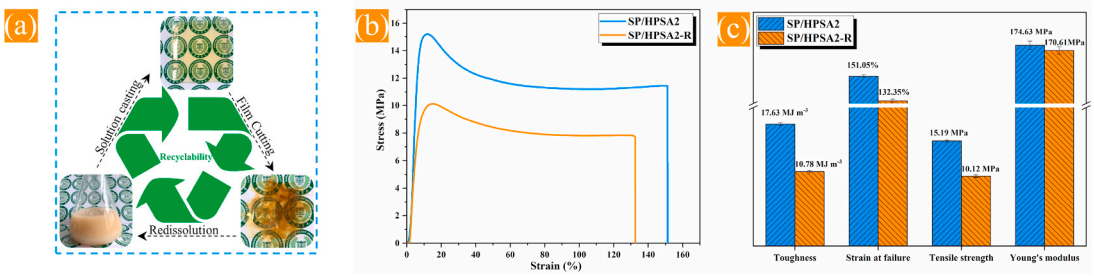

Fig. 4. (a) Illustration for the recycling performance of the as-fabricated films. (b) Engineering stress-strain curves of SP/HPSA2 and the recycled SP/HPSA2 (SP/HPSA2-R) films. (c) Toughness, strain at failure, tensile strength, and Young's modulus of SP/HPSA2 and SP/HPSA2-R films.

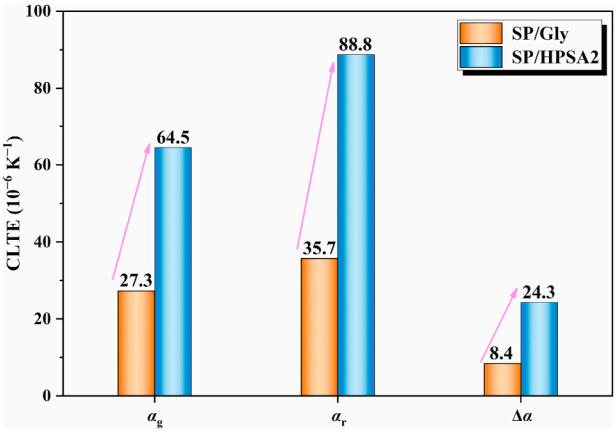

Fig. 5. (c) Coefficient of linear thermal expansion (CLTE) values of SP/Gly and SP/HPSA2 films.

3.6. Thermal performance

The thermal performance of the developed films was investigated by TGA, as shown in Fig. 7 and Fig. S6. For the SP/HPSA1 film, the temperature at the maximum thermal decomposition rate (T_{max}) increased to 275.7 °C from 271.2 °C for the SP/Gly film, and further increased with the HPSA loading content. The SP/HPSA5 film possessed the highest T_{max} of 291.0 °C, which was 19.8 °C increase compared with that of the SP/Gly film. The SP/Gly film possessed a low carbon yield at 600 °C (CY_{600}) of ca. 18.5%, while the SP/HPSA films exhibited higher CY_{600} of 28.5–29.8%, which was more than 10% higher than that of the SP/Gly film. The high thermal stability of the SP/HPSA film can be caused by the high heat-resistance properties of HPSA (Fig. S6) as well as the formation of strong interfacial interactions between HPSA and the protein matrix.

3.7. Fluorescent performance

Fig. 8a gives the photographs of 5 wt% SP and 5 wt% HPSA solutions under 365 nm UV illumination. As can be seen, the prepared HPSA was completely water soluble and the obtained HPSA solution can emit bright blue fluorescence. Conversely, the SP solution exhibited a very

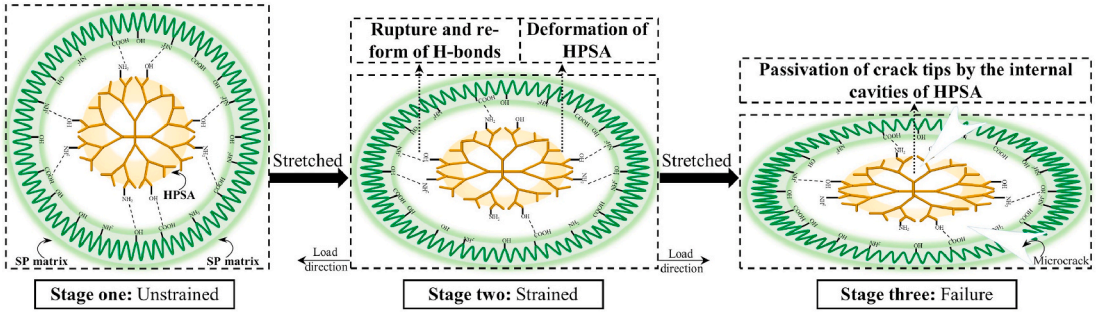

Fig. 6. The schematic representation of the toughening and reinforcing mechanism of HPSA in the SP matrix.

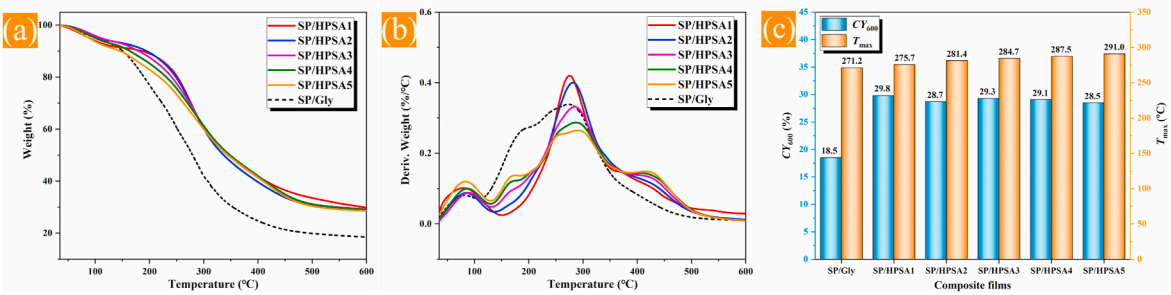

Fig. 7. (a) TGA and (b) DTG curves of SP/Gly, SP/HPSA1, SP/HPSA2, SP/HPSA3, SP/HPSA4, and SP/HPSA5 films. (c) The carbon yield at 600 °C (CY_{600}) and the temperature at the maximum thermal decomposition rate (T_{max}) of SP/Gly, SP/HPSA1, SP/HPSA2, SP/HPSA3, SP/HPSA4, and SP/HPSA5 films.

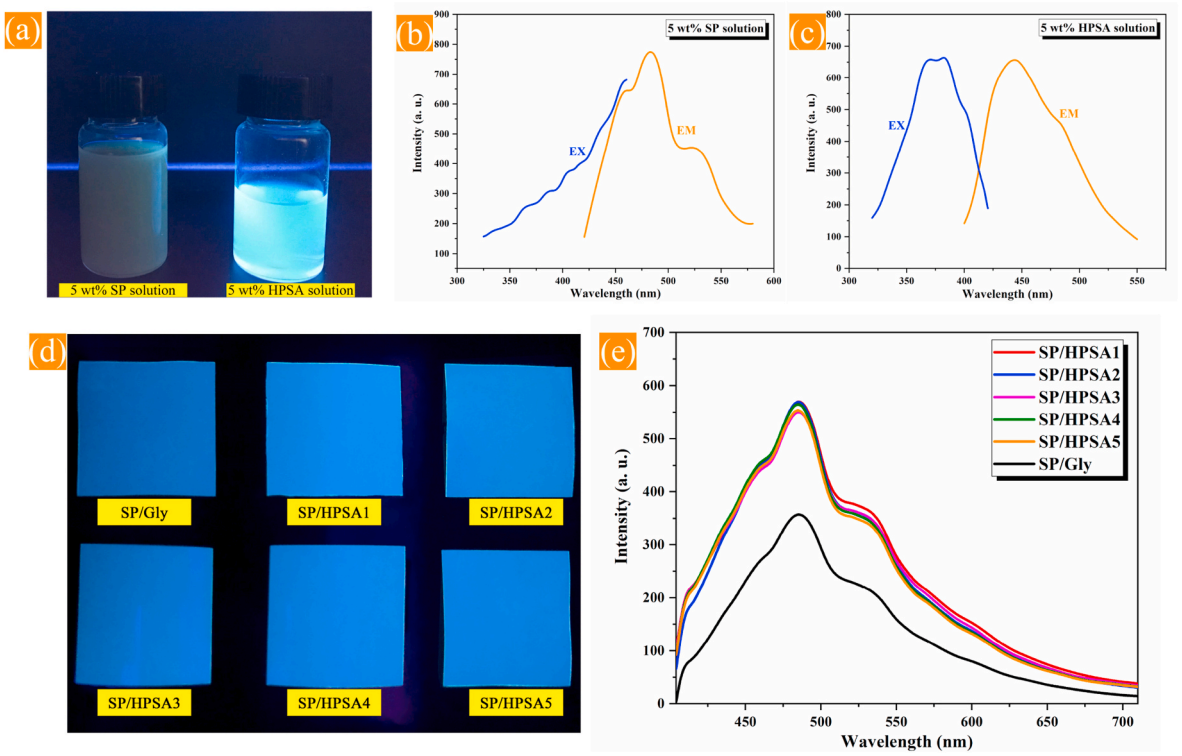

Fig. 8. (a) Photographs giving the fluorescence of 5 wt% SP and 5 wt% HPSA solutions under 365 nm UV illumination. Photoluminescence excitation (EX) and emission (EM) spectra of (b) 5 wt% SP solution and (c) 5 wt% HPSA solution. (d) Photographs giving the fluorescence of SP/Gly, SP/HPSA1, SP/HPSA2, SP/HPSA3, SP/HPSA4, and SP/HPSA5 films under 365 nm UV light. (e) Fluorescence spectra of SP/Gly, SP/HPSA1, SP/HPSA2, SP/HPSA3, SP/HPSA4, and SP/HPSA5 films.

light blue color inherent to the SP chains [5], revealing it possessed weak fluorescent properties. The photoluminescence excitation (EX) and emission (EM) spectra of the SP and HPSA solutions were acquired to further study their fluorescent properties (Fig. 8b and c). The SP and HPSA solutions possessed the EX bands at about 350–450 nm and 325–425 nm, and meanwhile held the EM bands at about 425–575 nm and 400–550 nm, respectively. The blue fluorescence emitted from HPSA was possibly caused by the emergence of hydroxyl group-rich nanocluster and electron-hole recombination processes corresponding the correlated electron-hole exciton states, or the radiative tunneling betwixt delocalized electrons and holes [25]. As shown in Fig. 8d, the SP/Gly film exhibited a light blue fluorescence, while the developed SP/HPSA films exhibited bright blue colors. In addition, the SP/Gly film exhibited a relatively weak fluorescence intensity, as can be seen in the fluorescence spectra (Fig. 8e). Nevertheless, strong EM bands concentrated at about 485 nm emerged in the fluorescence spectra of the SP/HPSA films, further confirming that the developed SP/HPSA films possessed strong blue fluorescence. Notably, the fluorescence intensity slightly decreased as the HPSA loading content, which was probably caused by the luminescence concentration quenching.

3.8. Biodegradable properties

Aqueous soil culture liquid method was used to determine the biodegradable properties of the prepared films according to previous works [5,22]. The weight residue profiles of different films after degradation are shown in Fig. 9a. As can be seen, the weight residue of all the films decreased dramatically over time, and decreased by more than 80% after 28 days, indicating that the developed films possessed great biodegradability. Moreover, the degraded films were seriously eroded and became fragmented (Fig. 9b), which further confirmed the excellent biodegradability of all the films. The solid content percentage

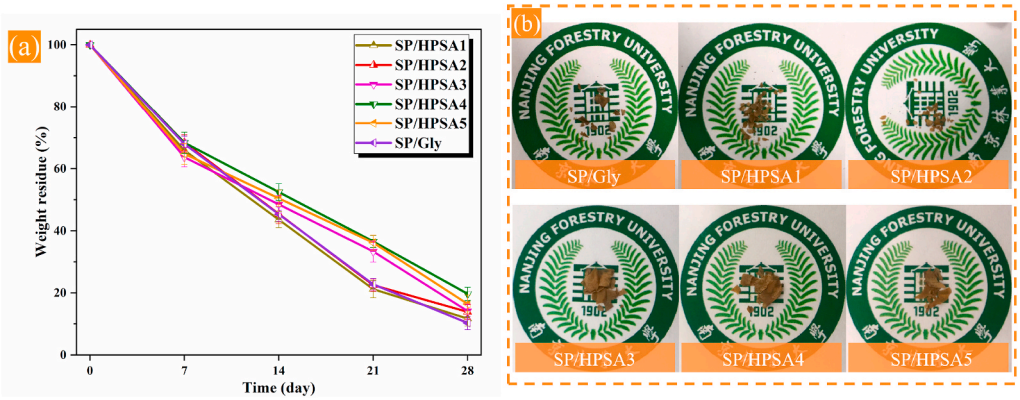

Fig. 9. (a) Weight residue profiles of SP/Gly, SP/HPSA1, SP/HPSA2, SP/HPSA3, SP/HPSA4, and SP/HPSA5 films degraded using aqueous soil culture liquid method. (b) Photographs of the fragmented films after degradation.

(SCP) of each component before degradation and the average total degraded weight percentage (TDWP) after degradation in different films were calculated to further investigated the biodegradable properties of the films (Table S2). For the films with HPSA loading content over 20%, the TDWP was higher than the SCP of HPSA and SP before the degradation, and the final weight residue was lower than the SCP of both HPSA and SP, which demonstrated that HPSA and the protein matrix must have been degraded [5]. For the SP/Gly film, the TDWP was higher than the SCP of glycerol and SP before the degradation, revealing that glycerol and the protein matrix must have been degraded [5]. In the light of the above results, the hybrid of HPSA and SP offers an effective and simple strategy for fabricating mechanically robust, recyclable, and fluorescent composite films with high thermal stability and good biodegradability. These merits make the developed composite films can be used to prepare high-performance, high-transparency, and anti-counterfeiting composites, which have promising applications in packaging materials.

4. Conclusions

A facile method was presented for fabricating tough, strong, recyclable, and biodegradable films with high thermal stability and fluorescent properties by simple solution casting of SP and HPSA. The fabricated SP/HPSA2 film possessed a high toughness of 17.63 MJ m^{-3} and a high tensile strength of 15.19 MPa, which was 424.70% and 551.93% increase compared with the 3.36 MJ m^{-3} and 2.33 MPa of the SP/Gly film, respectively. In addition, the SP/HPSA2 films also possessed a large strain at failure of 151.01%. A toughening and reinforcing mechanism associated with the strain-induced deformation and 3D enmeshment effect of HPSA on SP matrix was proposed. Incorporating the heat-resistant HPSA in SP significantly increased the CY_{600} and the T_{max} from 18.5% to 190.0 °C to 29.8% and 291.0 °C, respectively. Additionally, the developed composite films exhibited good recyclability due to the reversibility of the dynamic hydrogen bonds confined in the interphase, as well as great fluorescent properties because of the presence of fluorescent HPSA. This work offers a facile and effective strategy for fabricating mechanically robust, recyclable, and fluorescent composite films with high thermal stability and good biodegradable properties, which can be used for many promising applications like high-performance, high-transparency, and anti-counterfeiting packaging materials.

Credit authorship contribution statement

Jiongjiong Li: Investigation, Methodology, Data curation, Writing - original draft, Project administration. Shuaicheng Jiang: Data curation, Formal analysis. Ying Zhou: Formal analysis, Software. Xiaona Li: Data curation, Formal analysis. Sheldon Q. Shi: Visualization, Writing - review & editing. Jianzhang Li: Conceptualization, Methodology, Investigation, Writing - review & editing, Supervision.

Declaration of competing interest

The authors declare that they have no known competing financial interests or personal relationships that could have appeared to influence the work reported in this paper.

Acknowledgements

This study was financially supported by the Natural Science Foundation of Jiangsu Province (No. BK20200795) and the Scientific Research Start-up Funds of Nanjing Forestry University (No. 163020208).

Appendix A. Supplementary data

Supplementary data to this article can be found online at https://doi.org/10.1016/j.polymertesting.2021.107162.

References

[1] X. Zhang, W.F. Liu, D.J. Yang, X.Q. Qiu, Biomimetic supertough and strong biodegradable polymeric materials with improved thermal properties and excellent UV-blocking performance, Adv. Funct. Mater. 29 (2019) 1806912.
[2] P.W. Xu, W.J. Yang, D.Y. Niu, M.M. Yu, M.L. Du, W.F. Dong, M.Q. Chen, P. Jan Lemstra, P.M. Ma, Multifunctional and robust polyhydroxyalkanoate nanocomposites with superior gas barrier, heat resistant and inherent antibacterial performances, Chem. Eng. J. 382 (2020) 122864.
[3] H. Moustafa, A.M. Youssef, N.A. Darwish, A.I. Abou-Kandil, Eco-friendly polymer composites for green packaging: future vision and challenges, Compos. B Eng. 172 (2019) 16–25.
[4] K. Li, S. Jin, H. Chen, J. Li, Bioinspired interface engineering of gelatin/cellulose nanofibrils nanocomposites with high mechanical performance and antibacterial properties for active packaging, Compos. B Eng. 171 (2019) 222–234.
[5] Z. Chang, S. Zhang, F. Li, Z. Wang, J. Li, C. Xia, Y. Yu, L. Cai, Z. Huang, Self-healable and biodegradable soy protein-based protective functional film with low cytotoxicity and high mechanical strength, Chem. Eng. J. 404 (2020) 126505.
[6] W. Gu, F. Li, X. Liu, Q. Gao, S. Gong, J. Li, S.Q. Shi, Borate chemistry inspired by cell walls converts soy protein into high-strength, antibacterial, flame-retardant adhesive, Green Chem. 22 (2020) 1319–1328.
[7] B. Zhang, Z. Chang, J. Li, X. Li, Y. Kan, Z. Gao, Effect of kaolin content on the performances of kaolin-hybridized soybean meal-based adhesives for wood composites, Compos. B Eng. 173 (2019) 106919.
[8] Y. Han, K. Li, H. Chen, J. Li, Properties of soy protein isolate biopolymer film modified by graphene, Polymers 9 (2017) 312.
[9] H.J. Kang, X.S. Song, Z. Wang, W. Zhang, S.F. Zhang, J.Z. Li, High-performance and fully renewable soy protein isolate-based film from microcrystalline cellulose via bio-inspired poly(dopamine) surface modification, ACS Sustain. Chem. Eng. 4 (2016) 4354–4360.
[10] A. Xiang, G. Guo, H. Tian, Fabrication and properties of acid treated carbon nanotubes reinforced soy protein nanocomposites, J. Polym. Environ. 25 (2016) 519–525.
[11] S. Zhang, C. Xia, Y. Dong, Y. Yan, J. Li, S.Q. Shi, L. Cai, Soy protein isolate-based films reinforced by surface modified cellulose nanocrystal, Ind. Crop. Prod. 80 (2016) 207–213.
[12] W. Wang, F. Wang, C. Zhang, Z. Wang, J. Tang, X. Zeng, X. Wan, Robust, reprocessable, and reconfigurable cellulose-based multiple shape memory polymer enabled by dynamic metal-ligand bonds, ACS Appl. Mater. Interfaces 12 (2019), 25233-23242.
[13] C.H. Li, J.L. Zuo, Self-healing polymers based on coordination bonds, Adv. Mater. (2019), 1903762.
[14] M.G. Mazzotta, A.A. Putnam, M.A. North, J.J. Wilker, Weak bonds in a biomimetic adhesive enhance toughness and performance, J. Am. Chem. Soc. 142 (2020) 4762–4768.
[15] X. Wu, J. Wang, J. Huang, S. Yang, Robust, stretchable, and self-healable supramolecular elastomers synergistically cross-linked by hydrogen bonds and coordination bonds, ACS Appl. Mater. Interfaces 11 (2019) 7387–7396.
[16] Z. Wang, L. Guo, H. Xiao, H. Cong, S. Wang, A reversible underwater glue based on photo- and thermo-responsive dynamic covalent bonds, Materials Horizons 7 (2020) 282–288.
[17] L. Han, M. Wang, L.O. Prieto-López, X. Deng, J. Cui, Self-hydrophobization in a dynamic hydrogel for creating nonspecific repeatable underwater adhesion, Adv. Funct. Mater. 30 (2019) 1907064.
[18] W. Huang, D. Restrepo, J.-Y. Jung, F.Y. Su, Z. Liu, R.O. Ritchie, J. McKittrick, P. Zavattieri, D. Kisailus, Multiscale toughening mechanisms in biological materials and bioinspired designs, Adv. Mater. 31 (2019) 1901561.
[19] L. Gu, Y.Z. Jiang, J.L. Hu, Scalable spider-silk-like supertough fibers using a pseudoprotein polymer, Adv. Mater. 31 (2019) 1904311.
[20] W.W. Niu, Y.L. Zhu, R. Wang, Z.Y. Lu, X.K. Liu, J.Q. Sun, Remalleable, healable, and highly sustainable supramolecular polymeric materials combining superhigh strength and ultrahigh toughness, ACS Appl. Mater. Interfaces 12 (2020) 30805–30814.
[21] H. Wang, H. Liu, Z. Cao, W. Li, X. Huang, Y. Zhu, F. Ling, H. Xu, Q. Wu, Y. Peng, B. Yang, R. Zhang, O. Kessler, G. Huang, J. Wu, Room-temperature autonomous self-healing glassy polymers with hyperbranched structure, Proc. Natl. Acad. Sci. U.S.A. 117 (2020) 11299–11305.
[22] W. Gu, X. Liu, F. Li, S.Q. Shi, C. Xia, W. Zhou, D. Zhang, S. Gong, J. Li, Tough, strong, and biodegradable composite film with excellent UV barrier performance comprising soy protein isolate, hyperbranched polyester, and cardanol derivative, Green Chem. 21 (2019) 3651–3665.
[23] J.H. Zhang, S.Y. Chen, B. Qin, D.H. Zhang, P. Guo, Q.J. He, Preparation of hyperbranched polymeric ionic liquids for epoxy resin with simultaneous improvement of strength and toughness, Polymer 164 (2019) 154–162.
[24] Z. Wang, S.J. Zhao, H.W. Pang, W. Zhang, S.F. Zhang, J.Z. Li, Developing eco-friendly high-strength soy adhesives with improved ductility through multiphase core-shell hyperbranched polysiloxane, ACS Sustain. Chem. Eng. 7 (2019) 7784–7794.

[25] S. Niu, H. Yan, Z. Chen, L. Yuan, T. Liu, C. Liu, Water-soluble blue fluorescence-emitting hyperbranched polysiloxanes simultaneously containing hydroxyl and primary amine groups, Macromol. Rapid Commun. 37 (2016) 136–142.
[26] W. Gu, X. Liu, Q. Gao, S. Gong, J. Li, S.Q. Shi, Multiple hydrogen bonding enables strong, tough, and recyclable soy protein films, ACS Sustain. Chem. Eng. 8 (2020) 7680–7689.
[27] S.J. Zhao, Z. Wang, H.J. Kang, W. Zhang, J.Z. Li, S.F. Zhang, L. Li, A.M. Huang, Construction of bioinspired organic-inorganic hybrid composite by cellulose-induced interfacial gelation assisted with Pickering emulsion template, Chem. Eng. J. 359 (2019) 275–284.
[28] F. Li, Q.Q. Ye, Q. Gao, H. Chen, S.Q. Shi, W.R. Zhou, X.N. Li, C.L. Xia, J.Z. Li, Facile fabrication of self-healable and antibacterial soy protein-based films with high mechanical strength, ACS Appl. Mater. Interfaces 11 (2019) 16107–16116.
[29] S. Niu, H. Yan, Z. Chen, S. Li, P. Xu, X. Zhi, Unanticipated bright blue fluorescence produced from novel hyperbranched polysiloxanes carrying unconjugated carbon–carbon double bonds and hydroxyl groups, Polym. Chem-UK 7 (2016) 3747–3755.
[30] S.J. Zhao, Z. Wang, Z. Li, L. Li, J.Z. Li, S.F. Zhang, Core-shell nanohybrid elastomer based on co-deposition strategy to improve performance of soy protein adhesive, ACS Appl. Mater. Interfaces 11 (2019) 32414–32422.
[31] Z. Wang, S. Zhao, R. Song, W. Zhang, S. Zhang, J. Li, The synergy between natural polyphenol-inspired catechol moieties and plant protein-derived bio-adhesive enhances the wet bonding strength, Sci. Rep. 7 (2017) 9664.
[32] X. Xu, L. Jiang, Z. Zhou, X. Wu, Y. Wang, Preparation and properties of electrospun soy protein isolate/polyethylene oxide nanofiber membranes, ACS Appl. Mater. Interfaces 4 (2012) 4331–4337.
[33] Z. Wang, S.J. Zhao, H.J. Kang, W. Zhang, S.F. Zhang, J.Z. Li, Mussel byssus-inspired engineering of synergistic nanointerfacial interactions as sacrificial bonds into carbon nanotube-reinforced soy protein/nanofibrillated cellulose nanocomposites: versatile mechanical enhancement, Appl. Surf. Sci. 434 (2018) 1086–1100.
[34] S. Jin, K. Li, Q. Gao, W. Zhang, H. Chen, J. Li, Development of conductive protein-based film reinforced by cellulose nanofibril template-directed hyperbranched copolymer, Carbohydr. Polym. 237 (2020) 116141.
[35] J. Han, S.H. Shin, K.M. Park, K.M. Kim, Characterization of physical, mechanical, and antioxidant properties of soy protein-based bioplastic films containing carboxymethylcellulose and catechin, Food Sci. Biotechnol. 24 (2015) 939–945.
[36] M. Martelli-Tosi, M.M. Masson, N.C. Silva, B.S. Esposto, T.T. Barros, O.B.G. Assis, D.R. Tapia-Blacido, Soybean straw nanocellulose produced by enzymatic or acid treatment as a reinforcing filler in soy protein isolate films, Carbohydr. Polym. 198 (2018) 61–68.
[37] J. Wu, Q. Sun, H. Huang, Y. Duan, G. Xiao, T. Le, Enhanced physico-mechanical, barrier and antifungal properties of soy protein isolate film by incorporating both plant-sourced cinnamaldehyde and facile synthesized zinc oxide nanosheets, Colloids Surf. B Biointerfaces 180 (2019) 31–38.
[38] G. Guo, H. Tian, Q. Wu, Influence of pH on the structure and properties of soy protein/montmorillonite nanocomposite prepared by aqueous solution intercalating, Appl. Clay Sci. 171 (2019) 14–19.
[39] H. Xu, M. Yang, X. Hou, W. Li, X. Su, Y. Yang, Industrial trial of high-quality all green sizes composed of soy-derived protein and glycerol, J. Clean. Prod. 135 (2016) 1–8.
[40] B.S. Shim, J. Zhu, E. Jan, K. Critchley, S. Ho, P. Podsiadlo, K. Sun, N.A. Kotov, Multiparameter structural optimization of single-walled carbon nanotube composites: toward record strength, stiffness, and toughness, ACS Nano 3 (2009) 1711–1722.
[41] H. Lee, J. You, H.J. Jin, H.W. Kwak, Chemical and physical reinforcement behavior of dialdehyde nanocellulose in PVA composite film: a comparison of nanofiber and nanocrystal, Carbohydr. Polym. 232 (2020) 115771.
[42] N. Nordin, S.H. Othman, S.A. Rashid, R.K. Basha, Effects of glycerol and thymol on physical, mechanical, and thermal properties of corn starch films, Food Hydrocolloids 106 (2020) 105884.
[43] X. Sun, S. Sui, C. Ference, Y. Zhang, S. Sun, N. Zhou, W. Zhu, K. Zhou, Antimicrobial and mechanical properties of beta-cyclodextrin inclusion with essential oils in chitosan films, J. Agric. Food Chem. 62 (2014) 8914–8918.
[44] J. Shi, W. Liu, X. Jiang, W. Liu, Preparation of cellulose nanocrystal from tobacco-stem and its application in ethyl cellulose film as a reinforcing agent, Cellulose 27 (2020) 1393–1406.
[45] M.A.S.P. Nur Hazirah, M.I.N. Isa, N.M. Sarbon, Effect of xanthan gum on the physical and mechanical properties of gelatin-carboxymethyl cellulose film blends, Food Packaging and Shelf Life 9 (2016) 55–63.
[46] H. Sadeghifar, R. Venditti, J. Jur, R.E. Gorga, J.J. Pawlak, Cellulose-lignin biodegradable and flexible UV protection film, ACS Sustain. Chem. Eng. 5 (2016) 625–631.
[47] M. Yadav, S. Ahmad, F.-C. Chiu, Graphene oxide dispersed polyvinyl chloride/alkyd green nanocomposite film: processing and physico-mechanical properties, J. Ind. Eng. Chem. 68 (2018) 246–256.
[48] Z. Qi, Y. Tan, L. Gao, C. Zhang, L. Wang, C. Xiao, Effects of hyperbranched polyamide functionalized graphene oxide on curing behaviour and mechanical properties of epoxy composites, Polym. Test. 71 (2018) 145–155.